NANO LETTERS

pubs.acs.org/NanoLett Letter

Asynchronous-to-Synchronous Transition of Li Reactions in Solid-Solution Cathodes

Nikhil Sharma,[†] Luize Scalco de Vasconcelos,*[,†] Shadad Hassan, and Kejie Zhao*

Cite This: *Nano Lett.* 2022, 22, 5883−5890 Read Online

ACCESS | Metrics & More | Article Recommendations | Supporting Information

ABSTRACT: The composition dynamics regulate the accessible capacity and rate performance of rechargeable batteries. Heterogeneous Li reactions can lead to nonuniform electrochemical activities and amplify mechanical damage in the cell. Here, we employ *operando* optical microscopy as a laboratory tool to map the spatial composition heterogeneity in a solid-solution cathode for Li-ion batteries. The experiments are conducted at slow charging conditions to investigate the thermodynamic origins. We observe that the active particles charge asynchronously with reaction fronts propagating on the particle surfaces during the first charge, while subsequent (dis)charge cycles transition to a synchronous behavior for the same group of particles. Such transition is understood by computational modeling, which incorporates the dependence of Li diffusivity and interfacial reaction rate on the state of charge. The optical experiments and theoretical modeling provide insight into the reaction heterogeneity of porous electrodes and electrochemical conditioning for layered oxide cathodes.

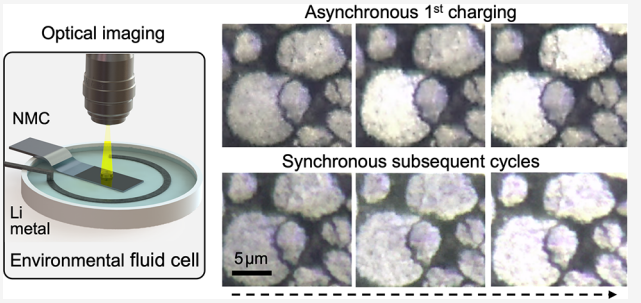

KEYWORDS: *Li kinetics, Li-ion battery, NMC, composition dynamics, layered oxide cathode, operando optical microscopy*

Nickel manganese cobalt oxides (NMCs) are the state-of-the-art cathode materials for Li-ion batteries thanks to their high voltage stability[1] and high energy density.[2] NMC materials,[3,4] as well as other similar layered transition metal oxides such as nickel cobalt aluminum oxides (NCAs),[5] suffer from a 10−30% capacity loss in the formation cycle, primarily attributed to the kinetic limitations rather than SEI formation.[6,7] Studies by Märker et al.[4] using *operando* synchrotron X-ray diffraction (XRD) and by Grenier et al.[5] using nuclear magnetic resonance (NMR) indicate that this kinetic limitation originates from an exceedingly low Li mobility at the fully lithiated state, which prevents complete reversal of the state-of-charge (SOC) at practical C-rates. Indeed, regardless of the material system, it follows Fick's law that a monotonically increasing diffusivity leads to an asymmetric rate-capability.[8] Grenier et al.[5] also observed that although NCA does not undergo a phase transition, a bimodal composition distribution appears during charging. Conversely, during discharging the Li distribution is homogeneous. A recent study by Park et al.[9] suggests that the bimodal distribution in non-phase transforming layered oxide cathodes may stem from a strong dependence of the interfacial reaction kinetics on Li concentration, giving rise to an autocalytic effect.[9] In addition to the first cycle capacity loss, nonuniform Li reactions can induce local structural damage.[10,11] In light of these observations, it is clear that the Li kinetics in solid solution materials can be nuanced, leading to short- and long-term consequences on the battery performance.

Although previous analyses showed bimodal composition dynamics in solid solution cathodes, several open questions remain: What is the length scale of the composition heterogeneity (interparticle or intraparticle)? How does this phenomenon progress over cycles at practical C-rates? Are existing theories sufficient to explain the mesoscale composition spatiodynamics across the electrode? This study employs *operando* optical microscopy paired with multiphysics modeling to answer these questions.

The easy access, low cost, and nondestructiveness of optical microscopy make it a suitable technique for conducting exhaustive and exploratory studies in Li-ion batteries[12] and has been gaining popularity in recent years.[13−15] In this work, the change in the reflected light intensity from an NMC cathode is tracked continuously over 3 days and used to infer the local composition change during slow charging over cycles, starting with the formation cycle. The dependence of the reflected light intensity on the Li content has been previously verified in a variety of active materials, including graphite,[16,17] silicon,[8,18] and $LiCoO_2$.[19] Our *operando* experiments reveal that NMC particles react asynchronously during the first

Received: May 5, 2022
Revised: June 26, 2022
Published: July 7, 2022

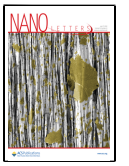

https://doi.org/10.1021/acs.nanolett.2c01818
Nano Lett. 2022, 22, 5883−5890

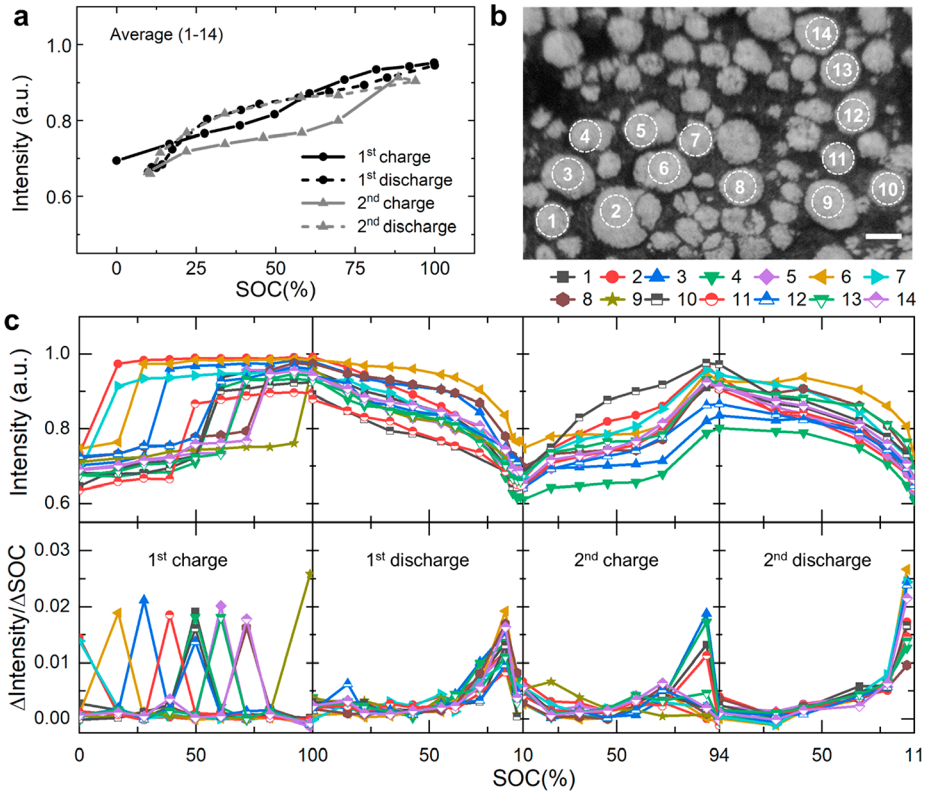

Figure 1. Pixel intensity of NMC particles in operando optical microscopy images across the first two cycles at C/20. (a) The average normalized pixel intensity of particles 1−14 marked in (b). The scale bar is 10 μm. The average intensity increases with delithiation (charging) and decreases with lithiation (discharging). (c) The normalized pixel intensity of individual particles (top panel) and corresponding slope (bottom panel). The first charge is characterized by an asynchronous step function (left plot in the top panel) and single peaks (left plot in the bottom panel). In contrast, subsequent (dis)charges proceed via a gradual, synchronous behavior.

charge of the formation cycle but transition toward uniform (synchronous) reactions in subsequent (dis)charge sequences. The numerical simulations show that solid-state diffusion alone cannot explain these observations and the phenomenon requires a spatially varying electric potential across the electrode surface. We show that the exceedingly low electrical conductivity of NMC in its pristine state and partial surface coverage of NMC by the conductive matrix can lead to such variation, producing the asynchronous reactions during the first charge. The transition to synchronous reactions happens naturally as a consequence of the incomplete composition reversal in the first cycle, which causes an increase in the baseline electrical conductivity and electric field homogenization. These findings suggest that improving the electrical conductivity of NMC and optimizing the conductive matrix coverage could prevent the first charge heterogeneous reactions and their detrimental consequences.

We record optical images of an NMC cathode inside a fluid cell with a Li metal anode upon cycling at a C-rate of C/20 (schematic in Figure S1). The NMC cathode is a polished composite electrode of $LiNi_{0.5}Mn_{0.3}Co_{0.2}O_2$ (NMC 532) active material particles, polymer binder, and carbon black conductive additive. We analyze the composition spatiodynamics of the electrode by the observed change in the reflected light intensity. Video S1 shows the time evolution of the optical images during the first two electrochemical cycles (~80 h). To quantify the change in the perceived brightness, we track the pixel intensity of 14 NMC particles (dashed circles in Figure 1b). The values of pixel intensity R+G+B (Red+Green+Blue) are measured in the range of 0−255 and normalized by 255. The average normalized intensity of the 14 particles as a function of the cell SOC is shown in Figure 1a. Note that there are certain limitations of the optical imaging technique such as the evolution of particle topography, small deviations in the lens focus, and a limited number of particles in the field of view. Therefore, the absolute difference in the average intensity at different charging states in Figure 1a is not so meaningful. Nevertheless, there is clear a correlation between intensity and SOC which suggests a monotonic dependence on Li content (i.e., an increase in intensity is directly proportional to a decrease in Li concentration). If we inspect individual particles instead of looking at the average intensity of all the particles, the intensity is widely nonuniform during the first charge. The top panel of Figure 1c shows that particles bright up abruptly and asynchronously (marked by sudden jumps in the intensity curves). These jumps in intensity do not occur in the following (dis)charge sequences despite the cell operating at the same C-rate (C/20). Instead, the intensity changes gradually with the SOC, indicating that all particles react at roughly the same time, and at a similar rate. The asynchronous-to-synchronous transition is most apparent when inspecting the slope of the intensity vs SOC curves (bottom panel of Figure 1c). For the first charge (left plot), the pristine particles are inactive for most of the SOCs (slope is practically zero throughout) except for one peak when the intensity abruptly switches from its baseline to its maximum value. This behavior is quite different in the following half-cycles, where particles react coherently (largely uniform Δintensity/ΔSOC). The voltage curve and optical images are summarized in Figure S2. This peculiar phenomenon happens across the entire surface electrode

https://doi.org/10.1021/acs.nanolett.2c01818
Nano Lett. 2022, 22, 5883−5890

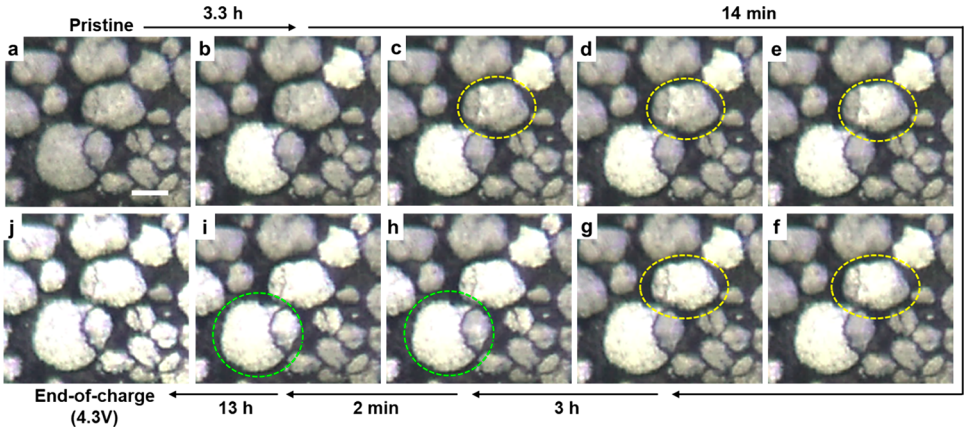

Figure 2. Operando optical images of the first charge (scale bar 10 μm) from (a) pristine state to (j) fully delithiated state in the course of 20 h. The individual sections of originally split particles (yellow and green dashed circles) delithiate at different times. The smaller fragments (likely having a worse electrical connection to the matrix) delithiate later.

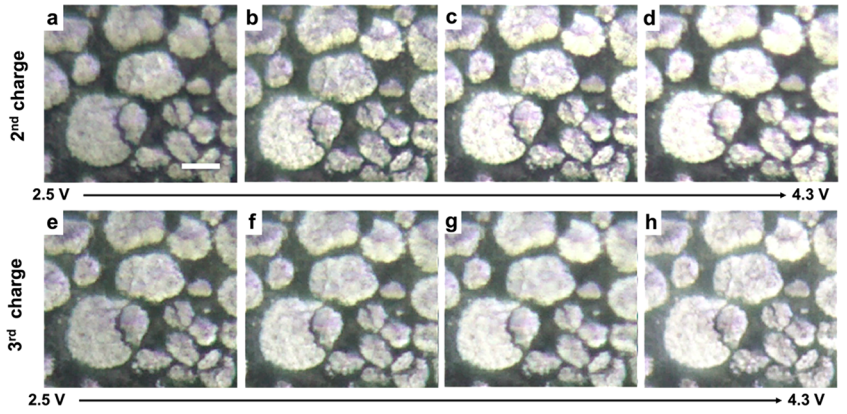

Figure 3. Operando optical images of the second (a–d) and third (e–h) charges (scale bar 10 μm). The uniform intensity change indicates that particles delithiate synchronously.

(optical images of different areas of the sample in Figure S3). Note that under the constant voltage step at the end of each (dis)charge sequence, there is a marked change in the intensity slope, which is likely a result of the surface saturating faster than the bulk under this condition.

To understand the intraparticle and interparticle composition spatiodynamics during the first charge, we inspect close-up optical images in Figure 2. Note that the two cracked particles enclosed by the yellow and green dashed lines were already damaged in their pristine state (Figure 2a), and their cracks are not a result of Li reactions. The images show that the intensity surge occurs at different stages of the first charge for particles belonging to the same neighborhood. For instance, the particle circled in yellow (Figure 2c) undergoes the intensity jump after 3.3 h into the charging process, while a neighboring particle (the smaller section of the particle enclosed by the green dashed circle, Figure 2h) does not react until 3.2 h later. Many surrounding particles display no sign of intensity change even after 13 h of charging (Figure 2i), and this interparticle heterogeneity exists throughout most of the operating range. The Li distribution appears to quickly homogenize within each particle (less than 14 min for the particle circled in yellow and 2 min for the right section of the cracked particle circled in green). We also note that the larger sections of the fragmented particles tend to react earlier than their counterparts. This observation may be related to the smaller sections having a worse connection to the electrically conductive carbon network of the cathode. Figure 3 of the second and third charges shows a different behavior from the first charge. The intensity change is gradual and uniform across and within all the particles indicating homogeneous composition dynamics.

We verify that this asynchronous Li deintercalation during the first charge also occurs for different NMC transition metal compositions ($LiNi_{0.8}Mn_{0.1}Co_{0.1}O_2$ - NMC811), electrolytes, and C-rates (see the list of supplementary experiments in Table S1, Figure S4, and S6). Notably, Figure 1a (potential w.r.t. SOC curve in Figure S2) shows that roughly 10% of the capacity is not recovered at the end of the first discharge, consistent with previous studies.[20,21] The capacity loss for the second cycle is negligible, providing a high Coulombic efficiency that is typically seen for NMC in the later cycles. Since we choose the operating voltage window of 4.3–2.5 V, we do not observe extensive structural degradation in the NMC532 particles (typically occurring at a higher voltage of 4.6 V[22,23] or a lower range of 1.7 V[24]). However, large cracks were observed in NMC811 particles even at moderate voltages (Figure S4). The fracture's timing correlated precisely with the intensity surge, which is further evidence of the intensity dependence on Li content.

The above results agree with previous observations made in similar materials[5] that a bimodal composition distribution exists during the first charge that does not show up during the

https://doi.org/10.1021/acs.nanolett.2c01818
Nano Lett. 2022, 22, 5883–5890

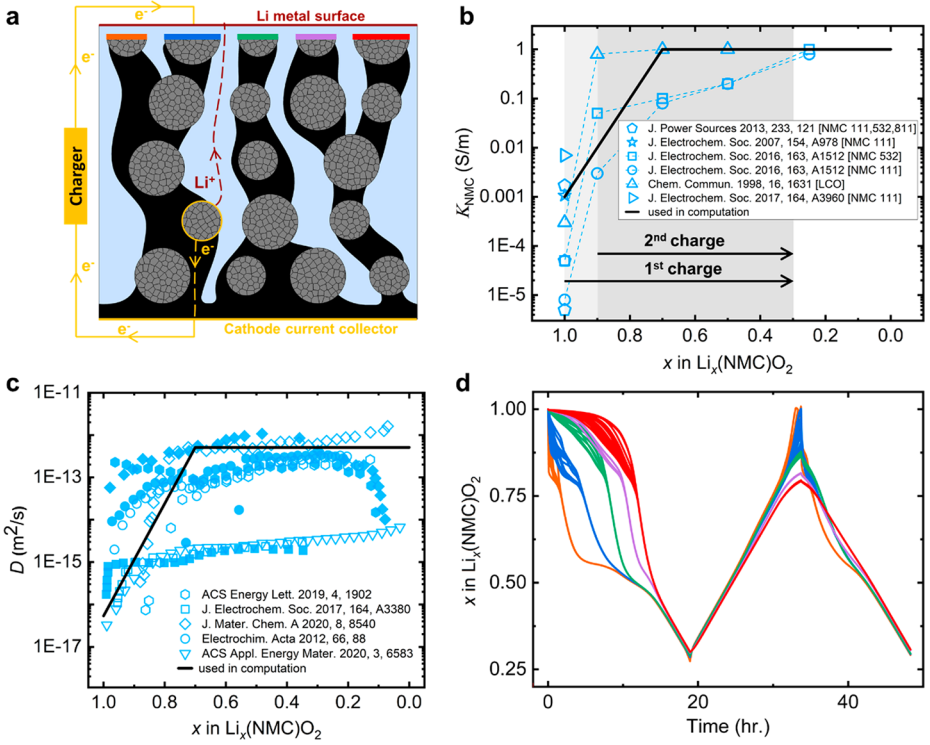

Figure 4. Schematic and parameters of computational modeling. (a) The 2D cathode cross-section geometry where polycrystalline NMC particles (gray) are embedded in a carbon network (black), surrounded by the electrolyte (light blue), and connected with a cathode current collector at the bottom. The interfacial reaction occurs at the NMC surface: in direct contact with the liquid electrolyte, and at the porous carbon binder interface. (b) Electrical conductivity (K_{NMC}) of NMC as a function of the SOC. The low value of K_{NMC} compared to that of carbon binder (~10^4 S/m) creates electrical resistance in the cathode leading to the asynchronous first charging behavior. The lower Li content at the first cycle compared to the pristine state leads to higher starting electrical conductivity for the following charge. This difference helps minimize the asynchronous behavior in later cycles at the same C-rate. (c) Diffusivity of NMC versus the SOC. The black curve is the curve used in the computational model. The low diffusivity in the low SOC region (x = 1.0−0.8 in $Li_x(NMC)O_2$) leads to capacity loss after the first cycle. (d) Li concentration at the color-coded locations on the surface of the topmost particles in (a) as a function of the charging time. Different colors are assigned to different secondary particles. The variation in the carbon conducting network to the topmost NMC particles results in an asynchronous charging only during the first charge, in agreement with the experimental results.

first discharge. However, we find that the earlier justification that the effect originates from Li mobility limitations is insufficient to explain the phenomenon observed here. In our experiment, the cathode is fully submerged in the electrolyte solution, and Li-ions are available throughout the entire surface of the particle being imaged. Thus, solid-state diffusion alone cannot explain the surface and interparticle heterogeneities. Hence, we further investigate this phenomenon using computational modeling to identify its underlying mechanism.

Consider the Butler−Volmer kinetics for the surface charge transfer at the interface of NMC and the liquid electrolyte

$$i_{BV} = i_0\left(\exp\left(\frac{\alpha_a F\eta}{RT}\right) - \exp\left(\frac{-\alpha_c F\eta}{RT}\right)\right) \quad (1)$$

$$\eta = \phi_s - \phi_l - E_{eq} \quad (2)$$

$$i_0 = F(k_c)^{\alpha_a}(k_a)^{\alpha_c}(c_{max} - c)^{\alpha_a}(c)^{\alpha_c}\left(\frac{c_l}{c_{l,ref}}\right)^{\alpha_a} \quad (3)$$

where i_{BV} is the redox current through the surface of the NMC particles, i_0 is the exchange current density, k_a and k_c are anodic and cathodic reaction rate constants, α_a and α_c are anodic and cathodic transfer coefficients, c_{max} is the maximum Li concentration in the active material, c is the Li concentration in the active material, F is the Faraday's number, c_l is the Li concentration in electrolyte, η is the electrochemical overpotential, ϕ_s is the local electric potential at the NMC particle reaction surface, ϕ_l is the local electrolyte potential, and E_{eq} is the equilibrium potential at a given local Li concentration when the active material and the electrolyte are at electrochemical equilibrium. The spatial variation of ϕ_s or ϕ_l for a thick cathode or during a high C-rate[11] can lead to dissimilar charging behavior of NMC particles. However, at the slow charging (C/20) condition, the spatial variation of ϕ_s or ϕ_l should be insignificant unless major electrical obstruction or ionic obstruction exists across the cathode.

The morphological features of the carbon binder network in commercial electrodes are generally heterogeneous: nonuniform distribution[25] and varying tortuosity[26] across the cathode, connectivity/dead ends,[27] and incomplete NMC particle coverage.[28] Because the NMC materials have electrical conductivity several orders of magnitude smaller than that of conductive carbon binder matrix,[29,30] one of the primary sources of obstruction to the electrically conductive network is the NMC particles. To simulate this effect, we create the 2D model depicted in Figure 4a with the NMC particles on the top surface (designated by orange, blue, green, purple, and red markings) experiencing varying degrees of electrical resistance from the conducting network. The rightmost particle (surface marked by the red line) experiences the largest degree of electrical obstruction with four NMC particles obstructing its

https://doi.org/10.1021/acs.nanolett.2c01818
Nano Lett. 2022, 22, 5883−5890

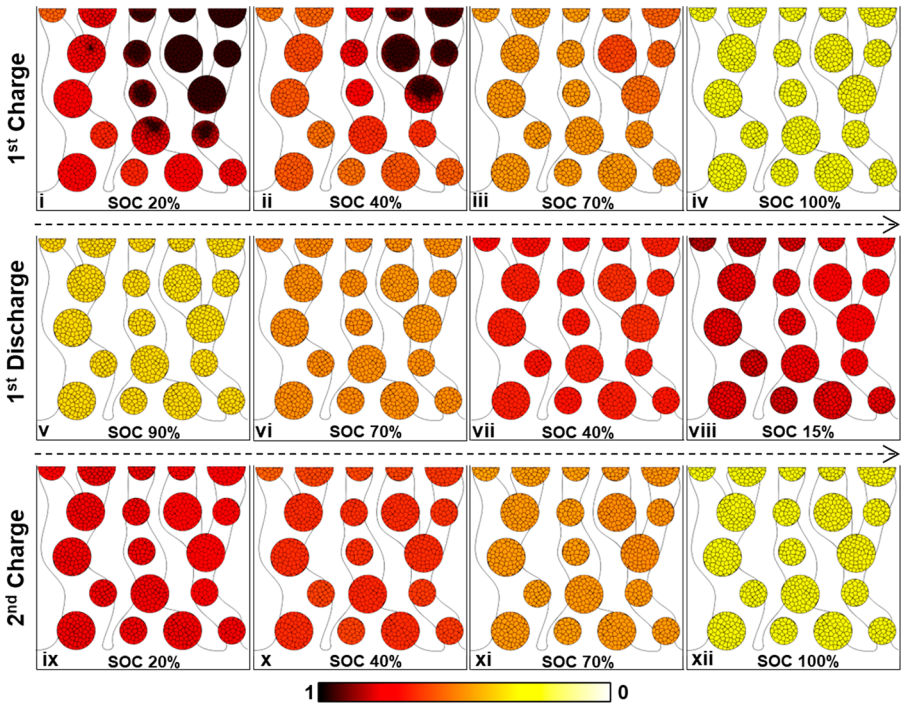

Figure 5. Computational modeling of the spatial distribution of Li in the NMC secondary particles. (a) Li profiles on the surface of the NMC particles at different states of charge. The first charge (first row) exhibits highly heterogeneous (intra- and interparticle) compositional dynamics where Li extraction starts from the pristine state (i) and ends at higher SOC on the right side (iv). The subsequent (dis)charges (second and third rows) show synchronous behavior.

conductive network. Conversely, the leftmost particle (surface marked by the orange line) has a direct carbon binder connection to the current connector. Depending on the magnitude of the electrical conductivity of the NMC particles, these differences in the conductive network will lead to spatial variations in the electric potential (ϕ_s), altering the local overpotential (η) and thus generating dissimilar interfacial currents (i_{BV}) at the NMC particle surfaces (based on eqs 1-(3)). Hence, the active particles in the same neighborhood but with different contacts with the conductive network can experience the onset of reactions at different times. Note that we do not intend to capture all the explicit microstructural details in a commercial composite cathode with the model in Figure 4a. Instead, the goal is to replicate the fact that the electrically conductive agent nonuniformly covers the active particles. The electrochemical modeling is based on the theory developed by Newman[31] in COMSOL. Note S1 and Tables S2−S4 show the governing equations, boundary conditions, and model parameters used in the calculations.

Li diffusivity in NMC is highly concentration-dependent as shown in Figure 4c (symbols represent literature data, and a continuous black line is the curve adopted in the model).[4,32−35] A general trend is that Li diffusivity in NMC is low at the start of charging ($x \sim 1$ in $Li_x(NMC)O_2$) and increases as the charging proceeds ($1 > x > 0.2-0.5$ in $Li_x(NMC)O_2$). This observation has a mechanistic explanation in terms of the divacancy diffusion mechanism where the Li mobility varies with the square of the number of vacancies.[5,36] In the case of silicon, we have previously demonstrated how the concentration-dependent diffusivity can create an intrinsically asymmetric performance during charging and discharging.[8] With the Li diffusivity increasing with the SOC, the time needed to fully discharge can be orders of magnitude higher than the charging time regardless of the type of boundary condition (Neumann/Dirichlet). For NMC, the lower diffusivity at high Li concentrations makes it challenging to reinsert all the Li back into the NMC lattice even at slow C-rates. After losing a fraction of the capacity at the end of the first cycle, the system stays at higher values of Li diffusivity for subsequent cycles, thus preventing further capacity loss in subsequent cycles. A similar trend holds for the reaction rate constant of NMC for the surface charge transfer.[37] A prior study showed that the variation of the reaction rate could result in the autocatalytic effect and fictitious phase separation in layered oxide cathode.[9]

Figure 4b shows literature reports[30,38−41] of the electrical conductivity of NMC materials (symbols) and the curve adopted in our computational model (continuous black line). The conductivity is several orders of magnitude lower in the pristine state than in the partially charged (delithiated) state.[39,41−43] This behavior is similar to $LiCoO_2$[44] and attributed to the transition from a semiconductor-like behavior to a metallic character caused by the initial Li removal.[40,45] Because of the capacity loss after the first cycle, the NMC particles will remain at a significantly higher electrical conductivity (in addition to higher diffusivity) for the start of the second charge (Figure 4b,c). Hence, we hypothesize that the low electrical conductivity of pristine NMC could explain the first charge asynchronous reactions. At the same time, the capacity loss is linked with the transition to synchronous reactions by preventing the NMC from reaching lower values of electrical conductivity (at a pristine state).

The model in Figure 4a is electrochemically cycled by enforcing a constant current at the Li source surface corresponding to a C-rate of C/20. Figure 4d shows the normalized surface concentration of Li with time for the

https://doi.org/10.1021/acs.nanolett.2c01818
Nano Lett. 2022, 22, 5883−5890

particles marked by different colors in Figure 4a. As per the hypothesis, the electrochemical activities are delayed with the increment of the electrical resistance along the path to the current collector (i.e., the leftmost top particle reacts first, and the rightmost top particle reacts last). This effect does not appear in the second charge because the incomplete Li intercalation at the end of the first cycle leads to the higher electrical conductivity at the start of the second charge (range indicated in the dark gray shade for the second charge in Figure 4b). In the absence of first cycle capacity loss, the asynchronous reactions would have continued into subsequent cycles. The spatial distribution of Li concentration is shown in the contour map of the NMC cathode in Figure 5. Because of the exceedingly low electrical conductivity of the NMC particles in the pristine state, the composition dynamics during the first charge are extremely sensitive to the characteristics of the carbon binder network. Low spatial interconnectivity of carbon binder within the electrode and incomplete coverage around NMC particle leads to highly heterogeneous Li distribution throughout the electrode. The intraparticle heterogeneity is also observed in a 3D single-particle model (Figure S5).

At the slow C/20 rate, it is worth noting that the reaction rate constant (k) contributes to the heterogeneity of the reactions in our model but not significantly (Figure S7). We do not consider any structural degradation of the NMC secondary particles in the computational study. Mechanical damage at the interphase of NMC and carbon binders, or the breakdown of the secondary particles, can further modulate the asynchronous reaction in the first charge, which we do not consider in the present study. The change in the carbon binder properties during (dis)charge,[46] interfacial debonding,[11,47] microstructural evolution of carbon binder network,[48] and particle crack generation[49,50] are vital occurrences during the first charge, which can regulate the asynchronous kinetics of NMC.

In conclusion, the *operando* optical microscopy affords an easily accessible yet powerful tool to observe the electrochemical behavior of multiple particles of the composite electrode in real -time. We present a study of the asynchronous reactions in a solid-solution cathode for Li-ion batteries during the first charge and the transition to the synchronous reactions in the following (dis)charge cycles. The mechanism is summarized as follows:

(1) The low electrical conductivity of NMC particles in the pristine state creates the spatial variation of the electric field and the reaction rate for the surface charge transfer. The carbon matrix's incomplete coverage of the NMC particles determines the intensity of reaction heterogeneity across the cathode during the first charge. Throughout the first discharge, the relatively higher values of electrical conductivity of NMC drastically diminish the heterogeneity.

(2) In agreement with previous studies, we find that the significant variation of Li diffusivity with Li concentration (orders of magnitude lower in the fully lithiated state) is responsible for the capacity loss at the end of the first cycle. Li diffusivity remains at a higher value at the start of the second charge.

(3) The incomplete Li intercalation after the first cycle promotes electrical conductivity of the NMC particles in subsequent cycles, resulting in homogeneous electrochemical activities throughout the composite cathode.

The mechanistic understanding is implemented in our 2D/3D models and can replicate the experimental observations. We assert that the asynchronous and synchronous Li activities are general phenomena for porous electrodes using layered metal oxide cathodes and are crucial factors determining rechargeable batteries' capacity and rate performance.

■ ASSOCIATED CONTENT

Supporting Information

The Supporting Information is available free of charge at https://pubs.acs.org/doi/10.1021/acs.nanolett.2c01818.

Details of methods, *operando* setup and experimental parameters, additional images of experiments, details of the theoretical model, and the parameters used in the computation modeling (PDF)

Optical microscopy video of NMC532 during the first two (dis)charge cycles at C/20 demonstrating asynchronous charging behavior during the first charge only; CC represents constant current (dis)charging; CV represents constant voltage (dis)charging (MP4)

First charge optical microscopy video of NMC532 in 1M LiPF6 in EC/DEC electrolyte at 100× optical microscope lens (Test 3 in Table S1) (MP4)

■ AUTHOR INFORMATION

Corresponding Authors

Kejie Zhao − *School of Mechanical Engineering, Purdue University, West Lafayette, Indiana 47907, United States;* orcid.org/0000-0001-5030-7412; Email: kjzhao@purdue.edu

Luize Scalco de Vasconcelos − *School of Mechanical Engineering, Purdue University, West Lafayette, Indiana 47907, United States;* orcid.org/0000-0002-4111-5619; Email: luizevasconcelos@utexas.edu

Authors

Nikhil Sharma − *School of Mechanical Engineering, Purdue University, West Lafayette, Indiana 47907, United States;* orcid.org/0000-0002-6441-8452

Shadad Hassan − *School of Mechanical Engineering, Purdue University, West Lafayette, Indiana 47907, United States*

Complete contact information is available at: https://pubs.acs.org/10.1021/acs.nanolett.2c01818

Author Contributions

N.S. and L.V. contributed equally to this work. L.V. and S.H. designed the experiments. N.S. and L.V. performed both the optical experiments and theoretical modeling. All of the authors wrote the paper. K.Z. supervised this work.

Author Contributions

†N.S. and L.S.V. contributed equally to this work.

Notes

The authors declare no competing financial interest.

■ ACKNOWLEDGMENTS

The authors are grateful for the support of the National Science Foundation through the Grants CMMI-1726392 and DMR-1832707.

■ REFERENCES

(1) Hu, M.; Pang, X.; Zhou, Z. Review Recent Progress in High-Voltage Lithium Ion Batteries. *J. Power Sources* **2013**, *237*, 229−242.

(2) Nitta, N.; Wu, F.; Lee, J. T.; Yushin, G. Li-Ion Battery Materials: Present and Future. *Mater. Today* **2015**, *18* (5), 252−264.
(3) Kasnatscheew, J.; Evertz, M.; Streipert, B.; Wagner, R.; Klöpsch, R.; Vortmann, B.; Hahn, H.; Nowak, S.; Amereller, M.; Gentschev, A. C.; Lamp, P.; Winter, M. The Truth about the 1st Cycle Coulombic Efficiency of $LiNi_{1/3}Co_{1/3}Mn_{1/3}O_2$ (NCM) Cathodes. *Phys. Chem. Chem. Phys.* **2016**, *18* (5), 3956−3965.
(4) Märker, K.; Reeves, P. J.; Xu, C.; Griffith, K. J.; Grey, C. P. Evolution of Structure and Lithium Dynamics in $LiNi_{0.8}Mn_{0.1}Co_{0.1}O_2$ (NMC811) Cathodes during Electrochemical Cycling. *Chem. Mater.* **2019**, *31* (7), 2545−2554.
(5) Grenier, A.; Reeves, P. J.; Liu, H.; Seymour, I. D.; Märker, K.; Wiaderek, K. M.; Chupas, P. J.; Grey, C. P.; Chapman, K. W. Intrinsic Kinetic Limitations in Substituted Lithium-Layered Transition-Metal Oxide Electrodes. *J. Am. Chem. Soc.* **2020**, *142* (15), 7001−7011.
(6) Kang, S. H.; Yoon, W. S.; Nam, K. W.; Yang, X. Q.; Abraham, D. P. Investigating the First-Cycle Irreversibility of Lithium Metal Oxide Cathodes for Li Batteries. *J. Mater. Sci.* **2008**, *43* (14), 4701−4706.
(7) Zhou, H.; Xin, F.; Pei, B.; Whittingham, M. S. What Limits the Capacity of Layered Oxide Cathodes in Lithium Batteries. *ACS Energy Lett.* **2019**, *4* (8), 1902−1906.
(8) de Vasconcelos, L. S.; Xu, R.; Zhao, K. Quantitative Spatiotemporal Li Profiling Using Nanoindentation. *J. Mech. Phys. Solids* **2020**, *144*, 104102.
(9) Park, J.; Zhao, H.; Kang, S. D.; Lim, K.; Chen, C. C.; Yu, Y. S.; Braatz, R. D.; Shapiro, D. A.; Hong, J.; Toney, M. F.; Bazant, M. Z.; Chueh, W. C. Fictitious Phase Separation in Li Layered Oxides Driven by Electro-Autocatalysis. *Nat. Mater.* **2021**, *20* (7), 991−999.
(10) Mendoza, H.; Roberts, S. A.; Brunini, V. E.; Grillet, A. M. Mechanical and Electrochemical Response of a $LiCoO_2$ Cathode Using Reconstructed Microstructures. *Electrochim. Acta* **2016**, *190*, 1−15.
(11) Xu, R.; Yang, Y.; Yin, F.; Liu, P.; Cloetens, P.; Liu, Y.; Lin, F.; Zhao, K. Heterogeneous Damage in Li-Ion Batteries: Experimental Analysis and Theoretical Modeling. *J. Mech. Phys. Solids* **2019**, *129* (2019), 160−183.
(12) Chen, B.; Zhang, H.; Xuan, J.; Offer, G. J.; Wang, H. Seeing Is Believing: In Situ/Operando Optical Microscopy for Probing Electrochemical Energy Systems. *Adv. Mater. Technol.* **2020**, *5* (10), 2000555.
(13) Maire, P.; Evans, A.; Kaiser, H.; Scheifele, W.; Novák, P. Colorimetric Determination of Lithium Content in Electrodes of Lithium-Ion Batteries. *J. Electrochem. Soc.* **2008**, *155* (11), A862.
(14) Harris, S. J.; Timmons, A.; Baker, D. R.; Monroe, C. Direct in Situ Measurements of Li Transport in Li-Ion Battery Negative Electrodes. *Chem. Phys. Lett.* **2010**, *485* (4−6), 265−274.
(15) Guo, Z.; Zhu, J.; Feng, J.; Du, S. Direct in Situ Observation and Explanation of Lithium Dendrite of Commercial Graphite Electrodes. *RSC Adv.* **2015**, *5* (85), 69514−69521.
(16) Maire, P.; Kaiser, H.; Scheifele, W.; Novák, P. Colorimetric Determination of Lithium-Ion Mobility in Graphite Composite Electrodes. *J. Electroanal. Chem.* **2010**, *644* (2), 127−131.
(17) Agrawal, S.; Bai, P. Operando Electrochemical Kinetics in Particulate Porous Electrodes by Quantifying the Mesoscale Spatiotemporal Heterogeneities. *Adv. Energy Mater.* **2021**, *11* (12), 2003344.
(18) Chen, J.; Yang, L.; Han, Y.; Bao, Y.-H.; Zhang, K.-L.; Li, X.; Pang, J.; Chen, H.-S.; Song, W.-L.; Wei, Y.-J.; Fang, D.-N. An in Situ System for Simultaneous Stress Measurement and Optical Observation of Silicon Thin Film Electrodes. *J. Power Sources* **2019**, *444*, 227227.
(19) Merryweather, A. J.; Schnedermann, C.; Jacquet, Q.; Grey, C. P.; Rao, A. Operando Optical Tracking of Single-Particle Ion Dynamics in Batteries. *Nature* **2021**, *594* (7864), 522−528.
(20) Weber, R.; Fell, C. R.; Dahn, J. R.; Hy, S. Operando X-Ray Diffraction Study of Polycrystalline and Single-Crystal $Li_xNi_{0.5}Mn_{0.3}Co_{0.2}O_2$. *J. Electrochem. Soc.* **2017**, *164* (13), A2992−A2999.
(21) Yu, Z.; Wang, H.; Kong, X.; Huang, W.; Tsao, Y.; Mackanic, D. G.; Wang, K.; Wang, X.; Huang, W.; Choudhury, S.; Zheng, Y.; Amanchukwu, C. V.; Hung, S. T.; Ma, Y.; Lomeli, E. G.; Qin, J.; Cui, Y.; Bao, Z. Molecular Design for Electrolyte Solvents Enabling Energy-Dense and Long-Cycling Lithium Metal Batteries. *Nat. Energy* **2020**, *5* (7), 526−533.
(22) Jung, R.; Metzger, M.; Maglia, F.; Stinner, C.; Gasteiger, H. A. Oxygen Release and Its Effect on the Cycling Stability of $LiNi_xMn_yCo_zO_2$ (NMC) Cathode Materials for Li-Ion Batteries. *J. Electrochem. Soc.* **2017**, *164* (7), A1361−A1377.
(23) Mao, Y.; Wang, X.; Xia, S.; Zhang, K.; Wei, C.; Bak, S.; Shadike, Z.; Liu, X.; Yang, Y.; Xu, R.; Pianetta, P.; Ermon, S.; Stavitski, E.; Zhao, K.; Xu, Z.; Lin, F.; Yang, X. Q.; Hu, E.; Liu, Y. High-Voltage Charging-Induced Strain, Heterogeneity, and Micro-Cracks in Secondary Particles of a Nickel-Rich Layered Cathode Material. *Adv. Funct. Mater.* **2019**, *29* (18), 1900247.
(24) Usubelli, C.; Besli, M. M.; Kuppan, S.; Jiang, N.; Metzger, M.; Dinia, A.; Christensen, J.; Gorlin, Y. Understanding the Overlithiation Properties of $LiNi_{0.6}Mn_{0.2}Co_{0.2}O_2$ Using Electrochemistry and Depth-Resolved X-Ray Absorption Spectroscopy. *J. Electrochem. Soc.* **2020**, *167* (8), 080514.
(25) Müller, M.; Pfaffmann, L.; Jaiser, S.; Baunach, M.; Trouillet, V.; Scheiba, F.; Scharfer, P.; Schabel, W.; Bauer, W. Investigation of Binder Distribution in Graphite Anodes for Lithium-Ion Batteries. *J. Power Sources* **2017**, *340*, 1−5.
(26) Ebner, M.; Chung, D. W.; García, R. E.; Wood, V. Tortuosity Anisotropy in Lithium-Ion Battery Electrodes. *Adv. Energy Mater.* **2014**, *4* (5), 1301278.
(27) Nguyen, T. T.; Villanova, J.; Su, Z.; Tucoulou, R.; Fleutot, B.; Delobel, B.; Delacourt, C.; Demortière, A. 3D Quantification of Microstructural Properties of $LiNi_{0.5}Mn_{0.3}Co_{0.2}O_2$ High-Energy Density Electrodes by X-Ray Holographic Nano-Tomography. *Adv. Energy Mater.* **2021**, *11* (8), 2003529.
(28) Jiang, Z.; Li, J.; Yang, Y.; Mu, L.; Wei, C.; Yu, X.; Pianetta, P.; Zhao, K.; Cloetens, P.; Lin, F.; Liu, Y. Machine-Learning-Revealed Statistics of the Particle-Carbon/Binder Detachment in Lithium-Ion Battery Cathodes. *Nat. Commun.* **2020**, *11* (1), 1−9.
(29) Chen, Y.-H.; Wang, C.-W.; Liu, G.; Song, X.-Y.; Battaglia, V. S.; Sastry, A. M. Selection of Conductive Additives in Li-Ion Battery Cathodes. *J. Electrochem. Soc.* **2007**, *154* (10), A978.
(30) Noh, H. J.; Youn, S.; Yoon, C. S.; Sun, Y. K. Comparison of the Structural and Electrochemical Properties of Layered $Li[Ni_xCo_yMn_z]O_2$ (x = 1/3, 0.5, 0.6, 0.7, 0.8 and 0.85) Cathode Material for Lithium-Ion Batteries. *J. Power Sources* **2013**, *233*, 121−130.
(31) Doyle, M.; Fuller, T. F.; Newman, J. Modeling of Galvanostatic Charge and Discharge of the Lithium/Polymer/Insertion Cell. *J. Electrochem. Soc.* **1993**, *140* (6), 1526−1533.
(32) Verma, A.; Smith, K.; Santhanagopalan, S.; Abraham, D.; Yao, K. P.; Mukherjee, P. P. Galvanostatic Intermittent Titration and Performance Based Analysis of $LiNi_{0.5}Co_{0.2}Mn_{0.3}O_2$ Cathode. *J. Electrochem. Soc.* **2017**, *164* (13), A3380−A3392.
(33) Hong, C.; Leng, Q.; Zhu, J.; Zheng, S.; He, H.; Li, Y.; Liu, R.; Wan, J.; Yang, Y. Revealing the Correlation between Structural Evolution and Li^+ Diffusion Kinetics of Nickel-Rich Cathode Materials in Li-Ion Batteries. *J. Mater. Chem. A* **2020**, *8* (17), 8540−8547.
(34) Yang, S.; Wang, X.; Yang, X.; Bai, Y.; Liu, Z.; Shu, H.; Wei, Q. Determination of the Chemical Diffusion Coefficient of Lithium Ions in Spherical $Li[Ni_{0.5}Mn_{0.3}Co_{0.2}]O_2$. *Electrochim. Acta* **2012**, *66*, 88−93.
(35) Jiang, M.; Zhang, Q.; Wu, X.; Chen, Z.; Danilov, D. L.; Eichel, R. A.; Notten, P. H. L. Synthesis of Ni-Rich Layered-Oxide Nanomaterials with Enhanced Li-Ion Diffusion Pathways as High-Rate Cathodes for Li-Ion Batteries. *ACS Appl. Energy Mater.* **2020**, *3* (7), 6583−6590.
(36) Van Der Ven, A.; Bhattacharya, J.; Belak, A. A. Understanding Li Diffusion in Li-Intercalation Compounds. *Acc. Chem. Res.* **2013**, *46* (5), 1216−1225.

https://doi.org/10.1021/acs.nanolett.2c01818
Nano Lett. 2022, 22, 5883−5890

(37) Ko, J. Y.; Varini, M.; Klett, M.; Ekström, H.; Lindbergh, G. Porous Electrode Model with Particle Stress Effects for Li-($Ni_{1/3}Co_{1/3}Mn_{1/3}$)O_2 Electrode. *J. Electrochem. Soc.* **2019**, *166* (13), A2939−A2949.
(38) Sauvage, F.; Tarascon, J. M.; Baudrin, E. In Situ Measurements of Li Ion Battery Electrode Material Conductivity: Application to Li_xCoO_2 and Conversion Reactions. *J. Phys. Chem. C* **2007**, *111* (26), 9624−9630.
(39) Amin, R.; Chiang, Y.-M. Characterization of Electronic and Ionic Transport in $Li_{1-x}Ni_{0.33}Mn_{0.33}Co_{0.33}O_2$(NMC 333) and $Li_{1-x}Ni_{0.50}Mn_{0.20}Co_{0.30}O_2$(NMC 523) as a Function Of. *J. Electrochem. Soc.* **2016**, *163* (8), A1512−A1517.
(40) Nishizawa, M.; Yamamura, S.; Itoh, T.; Uchida, I. Irreversible Conductivity Change of $Li_{1-x}CoO_2$ on Electrochemical Lithium Insertion/Extraction, Desirable for Battery Applications. *Chem. Commun.* **1998**, 1631−1632.
(41) Asano, T.; Yubuchi, S.; Sakuda, A.; Hayashi, A.; Tatsumisago, M. Electronic and Ionic Conductivities of $LiNi_{1/3}Mn_{1/3}Co_{1/3}O_2$-$Li_3PS_4$ Positive Composite Electrodes for All-Solid-State Lithium Batteries. *J. Electrochem. Soc.* **2017**, *164* (14), A3960−A3963.
(42) Wang, S.; Yan, M.; Li, Y.; Vinado, C.; Yang, J. Separating Electronic and Ionic Conductivity in Mix-Conducting Layered Lithium Transition-Metal Oxides. *J. Power Sources* **2018**, *393* (March), 75−82.
(43) Huddleston, W.; Dynys, F.; Sehirlioglu, A. Effects of Microstructure on Fracture Strength and Conductivity of Sintered NMC333. *J. Am. Ceram. Soc.* **2020**, *103* (3), 1527−1535.
(44) Shibuya, M.; Nishina, T.; Matsue, T.; Uchida, I. In Situ Conductivity Measurements of $LiCoO_2$ Film during Lithium Insertion/Extraction by Using Interdigitated Microarray Electrodes. *J. Electrochem. Soc.* **1996**, *143* (10), 3157−3160.
(45) Molenda, J.; Baster, D.; Milewska, A.; Swierczek, K.; Bora, D. K.; Braun, A.; Tobola, J. Electronic Origin of Difference in Discharge Curve between Li_xCoO_2 and Na_xCoO_2 Cathodes. *Solid State Ionics* **2015**, *271*, 15−27.
(46) Trembacki, B. L.; Noble, D. R.; Brunini, V. E.; Ferraro, M. E.; Roberts, S. A. Mesoscale Effective Property Simulations Incorporating Conductive Binder. *J. Electrochem. Soc.* **2017**, *164* (11), E3613−E3626.
(47) Liu, P.; Xu, R.; Liu, Y.; Lin, F.; Zhao, K. Computational Modeling of Heterogeneity of Stress, Charge, and Cyclic Damage in Composite Electrodes of Li-Ion Batteries. *J. Electrochem. Soc.* **2020**, *167* (4), 040527.
(48) Liu, H.; Foster, J. M.; Gully, A.; Krachkovskiy, S.; Jiang, M.; Wu, Y.; Yang, X.; Protas, B.; Goward, G. R.; Botton, G. A. Three-Dimensional Investigation of Cycling-Induced Microstructural Changes in Lithium-Ion Battery Cathodes Using Focused Ion Beam/Scanning Electron Microscopy. *J. Power Sources* **2016**, *306*, 300−308.
(49) Li, G.; Zhang, Z.; Huang, Z.; Yang, C.; Zuo, Z.; Zhou, H. Understanding the Accumulated Cycle Capacity Fade Caused by the Secondary Particle Fracture of $LiNi_{1-x-y}Co_xMn_yO_2$ Cathode for Lithium Ion Batteries. *J. Solid State Electrochem* **2017**, *21* (3), 673−682.
(50) Xu, R.; de Vasconcelos, L. S.; Shi, J.; Li, J.; Zhao, K. Disintegration of Meatball Electrodes for $LiNi_xMn_yCo_zO_2$ Cathode Materials. *Exp. Mech.* **2018**, *58* (4), 549−559.

https://doi.org/10.1021/acs.nanolett.2c01818
Nano Lett. 2022, 22, 5883−5890